iScience

CellPress
OPEN ACCESS

Review

Electro-, thermo-, and photocatalysis of versatile nanocomposites toward tandem process

Weikang Wang,[2,3] Jialun He,[1,3] Juan Deng,[1] Xiao Chen,[1] and Chao Yu[1,*]

SUMMARY

Tandem reactions involve multi-step processes conducted in one pot, offering a cost-effective, environmentally friendly, and efficient approach to chemical transformations with high atom economy. The catalytic systems employed in tandem reactions are crucial for achieving desirable activity, selectivity, and stability. Researchers worldwide have extensively explored catalytic processes driven by various energy fields, such as electrocatalysis, thermocatalysis, and photocatalysis, aiming to facilitate multiple reactions and bond transformations. Continuous advancements have been made in reaction conditions, catalyst design, and preparation methods. This review provides a comprehensive overview of recent progress in tandem reactions, specifically focusing on electro-, thermo-, and photocatalysis, and categorizes them into catalysts, reactors, and fields based on their applications. Furthermore, the review highlights the significance of rational design in nanomaterial catalysts and the integration of multiple energy sources, emphasizing their potential to enhance selectivity, performance, and the development of combined catalysis.

INTRODUCTION

In recent years, the industrial catalysis contributes to nearly 25% of the gross domestic product (GDP) in developed countries through synthesis processes or products.[1] Thereby, how to get rid of the useless byproduct or chemical wastes, reduce greenhouse gases output (CO_2, CH_4, etc.), and large energy consumption during traditional catalytic process comes out to be of great significance in social economic sustainable development. To transfer the current fossil fuel economy, including oil, coal, and natural gas, toward renewable and sustainable energy, variety of green and low-cost technologies, including different catalysis methods and modified chemical synthesis process, have soared in the last decades. Compared with traditional industrial catalysis, rational design of nano-scale catalysts and one-pot tandem reactions should be potential eco-friendly catalysis methods.

Tandem reactions or domino (cascade) reactions refers to accomplishing two or more successive bond-forming transformation reactions in a one-pot system without adding additional reagents and catalysts.[2] Different from cascade or domino reactions, more than one bond-forming transformation mechanism is required in sequential catalytic processes for tandem reactions.[3,4] Moreover, tandem reactions can be further divided into subcategories of orthogonal tandem reactions and auto/assisted tandem reactions based on the utilization of single precatalyst or chemical trigger, which has been discussed in detail in some previous reports.[5,6] For the synthesis of valuable products, tandem reaction pathway is an effective strategy to reduce the cost and environmental impact of chemical processes, as replacing step-by-step reactions with one-step or one-pot reaction leads to significant alleviation of the necessity of costly and harmful separation and purification processes.[7,8] Therefore, the tandem catalysis processes have been already applied in various catalytic fields.[9–11]

Besides the difference in number of catalytic mechanisms for one-pot system, various application scenarios of tandem reactions have been carried out by researchers all over the globe.[12,13] For example, to achieve orthogonal tandem catalysis, there should be a multiple-catalyst with more than one components in the one-pot system, accounting for different catalytic mechanisms, which can be defined as tandem catalysts.[13] Moreover, since reaction conditions are essential to catalytic processes, coupling more than one driving filed (including heat, electricity, and radiation) to promote different catalytic cycles can be recognized as tandem field.[14] Similarly, combining two or more reactors to realize tandem reactions can be labeled as tandem reactor.[15]

To clarify different application scenarios of tandem reactions, this review summarizes recent advances in tandem catalysis reactions driven by electric-, light-, heat-field, etc., and further classifies them as tandem catalysts, tandem field, and tandem reactor (Figure 1). Firstly, we provide a brief and comprehensive comparison of the fundamental aspects of traditional and emerging tandem reactions. In the second section, several advances of tandem reactions by electro-, thermo-, and photocatalysis process are outlined and divided into three classes based on application scenarios: tandem catalysts, tandem field, and tandem reactor. Finally, the last section summarizes some challenges and perspectives of tandem reactions for energy conversion field.

[1]School of Environmental and Chemical Engineering, Jiangsu University of Science and Technology, Zhenjiang, Jiangsu 212003, P.R. China
[2]School of Materials Science and Engineering, Jiangsu University, Zhenjiang, Jiangsu 212013, P.R. China
[3]These authors contributed equally
*Correspondence: chao_yu@just.edu.cn
https://doi.org/10.1016/j.isci.2024.108781

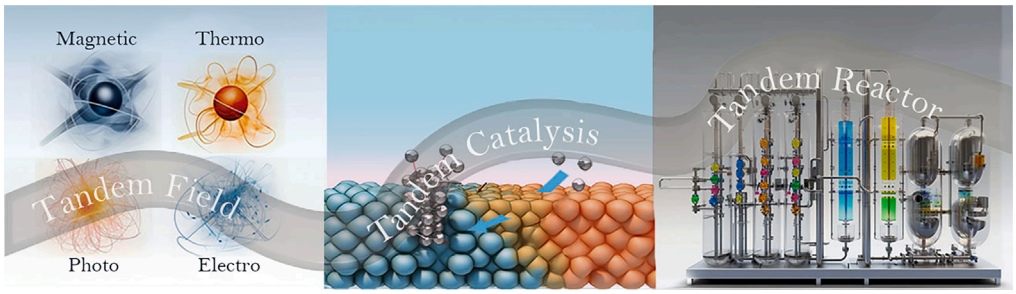

Figure 1. Diagram of tandem process

EMERGING TANDEM REACTIONS

Generally, there are three types of traditional coupling tandem reactions. The first type is that the reactants couple with new intermediates in the presence of catalyst. For instance, Yu et al. carried out a one-pot process with reactants and formic acid (HCOOH)-derived intermediates to realize the controlled polymerization and formation of target polymer products, including polybenzoxazole (PBO) and quinazoline.[16,17] The second type of traditional tandem reactions is typical coupling reaction with two or more same reactants, like CO_2 electrolysis toward multi-carbon fuels based on Cu-Ag tandem catalysts.[13] Indeed, accomplishing multiple-step reactions via a single catalytic mechanism or single type bond-forming transformations can be defined as domino (or cascade) reaction, rather than the tandem reaction. Differently, the type III of tandem reaction refers to different intermediates activated by corresponding catalyst toward coupling product, including two- (or multi-) component catalysts or a multifunctional catalyst; for example, Scott and Zhao immobilized the enzyme within a protective mesoporous silica, using a solid acid catalyst to minimize interactions with the enzyme, which can be recognized as tandem catalyst in this review.[18] In summary, the rational-designed tandem reaction can not only reduce the energy consumption and chemical waste but also minimize the applications of solvents and reagents.

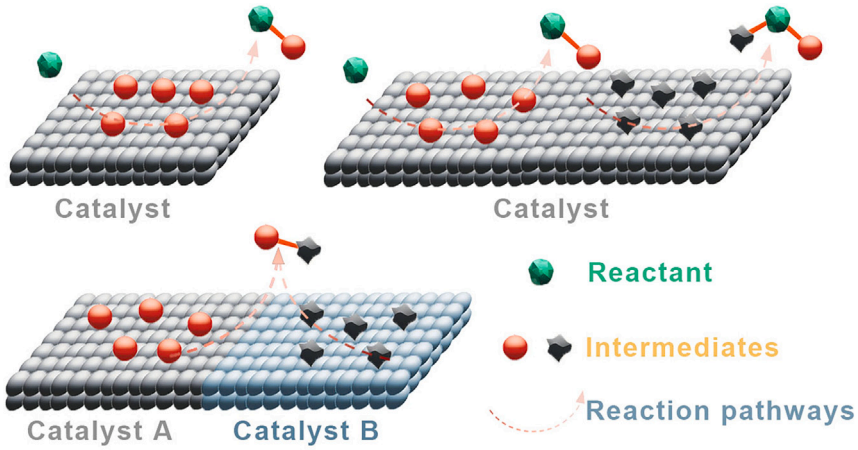

Diagram of three types of traditional coupling tandem reactions

Through screening catalysts with different structures and components based on experimental and theoretical results, a series of high-performance nanocatalysts for electrocatalysis, thermocatalysis, and photocatalysis strategies have been designed and formed by searchers to realize tandem reactions in recent years.[7,19,20] Herein, the emerging tandem reactions driven by different energy fields with variety of nanocatalysts will be comprehensively reviewed.

Electrocatalytic tandem reactions

As a rising start in heterogeneous catalysis, electrocatalysis driven by electric energy converted from renewable energy (including wind, solar, tidal energy, etc.) with various advantages has been regarded as an energy-saving and environmentally benign strategy for various redox reactions.[21,22] Considering the rapid development of electric conversion and storage, electrocatalysis process can be operated in a more stable condition without any environmental effect, unlike the negative effect of climate or sunlight change on photocatalysis.

The core concerns during electrocatalytic process can be distinguished as three aspects: 1) increasing Faradic efficiency (FE); 2) promoting selectivity and reducing byproducts; and 3) optimizing mass transport and diffusion of reactants and products. Correspondingly, substantial research effort has been devoted to enhance the electrocatalytic performance and focus on surface faceting, nano-structuring, heteroatom

Table 1. Electrocatalytic tandem reactions

Reaction	Catalyst	Condition	Reactivity	Year
CO_2 reduction into C_{2+}	Cu/ZnO tandem electrode	KOH electrolyte (1 M)	C_{2+} product (C_2H_4, C_2H_5OH) FE of 78% (−0.73 V vs. RHE)	2020 Zhang et al.[25]
Electrocatalytic C_2H_4 production from CO_2	nanodefective Cu nanosheets	CO_2-saturated 0.1 M K_2SO_4 electrolyte	C_2H_4 FE of 83.2% (−1.18 V vs. RHE)	2020 Zhang et al.[26]
C_{2+} products formation	Cu film coated PTFE membrane	0.05 M Cs_2CO_3 electrolyte, analysis by differential electrochemical mass spectroscopy	C_{2+} products FE of 81% (−1.15 V vs. RHE) under pulsed electrolysis	2020 Kim et al.[27]
Reduction of CO_2 to multi-carbon products	Cu-SA/NPC	CO_2-saturated 0.1 M $KHCO_3$ electrolyte solution (pH 6.8)	C_3H_6O FE of 36.7%, production rate of 336.1 μg h^{-1}	2020 Zhao et al.[28]
n-propanol formation from CO_2	activated PdCu alloy foam	0.5 M $KHCO_3$ electrolyte solution (pH 7.2)	*n*-propanol FE of 13.7% ($J = -1.15$ mA cm^{-2}) at −0.65 V vs. RHE	2020 Rahaman et al.[29]
Selective C_{2+} production reaction	sprayed powder Cu	0.1 M $KHCO_3$ electrolytes	C_2H_4 (FE $\leq$ 39%)	2020 Kim et al.[30]
Electrocatalytic CO_2 reduction toward C_2 products	Re-Cu-I	0.1 M $KHCO_3$ electrolytes (pH 6.8)	FE for C_2 species reaches 80% with a partial current density of 21 mA cm^{-2}	2020 Han et al.[31]
CO_2 electro-conversion to multi-carbons (C_{2+})	Cu-Ag tandem catalyst	1 M KOH electrolytes	6.43, 11.27 and 16.22 μg h^{-1} cm_{geom}^{-2} production rates toward C_2H_4, C_2H_5OH, and CH_3COO^-	2020 Chen et al.[13]
Electrochemical CO_2 reduction toward C_2 products	Cu nanocubes with 44 nm edge length	0.1 M $KHCO_3$ electrolytes	C_2H_4 FE of 41%, C_2H_4/CH_4 = 2.03–1.1 V vs. RHE	2016 Loiudice et al.[32]
C–C coupling of furfural and benzaldehyde				2020 Anibal and Xu[33]

doping, heterojunction, and electrolyte effects, and some of the state-of the-art progress has been previously summarized in several reviews.[23,24] In comparison with conventional electrocatalytic processes, the tandem reaction systems, featuring multiple active centers or porous architectures, emerge as a compelling approach to generating value-added products, especially in C1 chemistry where CO_2 is converted to multi-carbons (C_{2+}), as presented in Table 1 in the following. Traditional catalysts often grapple with challenges in achieving meticulous control over multi-interface catalyst composition and microstructure. This difficulty in controlling metal size, position, composition, and microenvironment, coupled with the inherent complexity of the structures, leads to the stringent reaction conditions, poor reaction selectivity, and consequently, the production of numerous byproducts, and substantial energy consumption in subsequent separation processes. On the other hand, tandem catalysts, by integrating multiple active sites on the catalyst, facilitate the coupling of several individual or intrinsically related proton-electron transfer steps to realize tandem reactions. This methodology holds promise in reducing chemical engineering costs through scalable and multi-tiered molecular utilization, thereby paving the way for more efficient and economically viable catalytic processes in the industry.

Lately, Wu and Weber et al. designed a segmented gas-diffusion electrode (Cu/Ag s-GDEs) with a CO-selective catalyst layer (CL) at the inlet to prolong the CO-residence time, which is in favor of subsequent C_{2+}-selective segment. Owing to the enhanced *CO coverage within the Cu CL, an optimal FE of C_{2+} reached 90% at C_{2+} partial current density (j_{C2+}) exceeding 1 A cm^{-2} by a Cu/Fe-N-C s-GDE.[34] As exhibited in Figure 2, different structures of stacked and coplanar s-GDEs with Ag and Cu CL segments were designed and fabricated. In both situations, the Ag CL aligns with the CO_2 inlet to enable effective conversion of continuous CO_2 for a supplementary CO supply, which promotes θ_{*CO} and can be transformed to C_{2+} products over the subsequent Cu CL (analogous to tandem reaction of $CO_2 \rightarrow CO \rightarrow C_2H_4$ in a plug-flow reactor, Figure 2D). In this work, the Ag and Cu CL segments were designed to take charge of CO residence and C–C coupling in a flow channel, which can be recognized as a typical tandem reactor.

However, majority of tandem reactions of conversion of CO_2 to C_{2+} product only proceed with one bond-transformation mechanism, prefering to meet the definition of domino or cascade reactions.[3,5] Besides the CO_2 upgrading reactions, the electroreductive coupling or C–C bond formation reaction is also typical tandem reactions, displaying attractive promise for larger, biomass-derived aldehydes

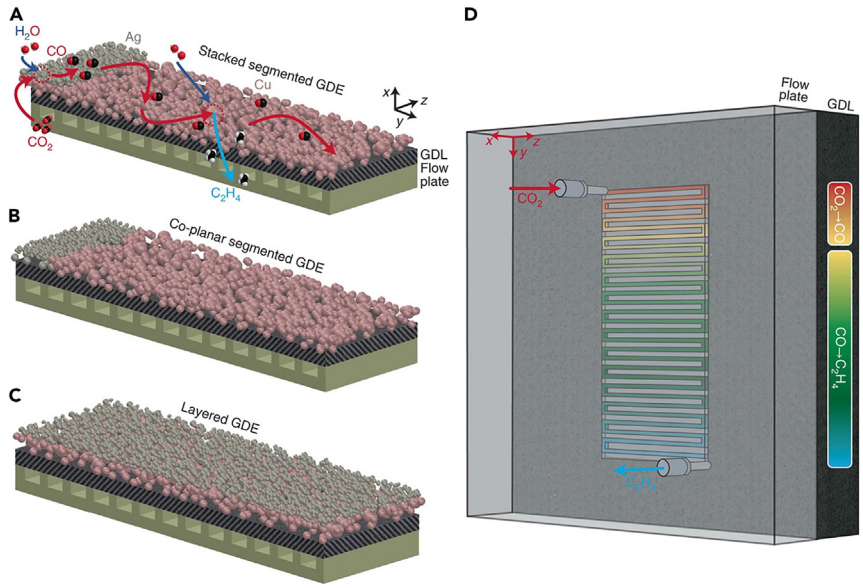

Figure 2. Diagram of segmented tandem GDEs

(A–C) Schematic of stacked (A) and coplanar (B) segmented GDEs. The structure of contrastive layered GDE is also displayed in the bottom panel (C). Diagram of the flow channel with changing gas concentration.

(D) Concept of segmented tandem gas-diffusion electrodes. Reproduced with permission from Zhang et al.[34]

(e.g., benzaldehyde and furfural derivatives). In 2020, Anibal and Xu investigated the electroreductive coupling of benzaldehyde and furfural on Cu and Pb electrodes.[33] Electrocatalytic performance studies revealed both self-coupling and cross-coupling of the two aldehydes on these two metal surfaces, but with different preference (Figure 3). It can be proved that the cross-coupling of two aldehydes follows a two reactant Sabatier rule, with optimum cross-coupling for electrodes and similar reactant binding energies. The fabricated Cu and Pb composite electrodes, accounting for greater selectivity for cross-coupling and furfural coupling, respectively, are typical tandem catalysts.

Coupling reaction of CO_2 with N_2 to form C–N bonds is a novel reaction path. As revealed in Figures 4A–4C, Wang and co-workers reported the directly coupled N_2 and CO_2 in H_2O to electrocatalytically synthesize urea under ambient conditions, employing PdCu alloy nanoparticles (NPs) on TiO_2 nanosheets as electrocatalyst.[35] The electrochemical results of FEs and corresponding current densities summarized in Figure 4D demonstrated that the urea formation rates in flow cells were substantially enhanced, reaching the highest yield rate of 3.36 mmol g^{-1} h^{-1} at −0.4 V (vs. RHE). The rational design of electrocatalyst endows it with enhanced chemisorption and catalytic activity for N_2 and CO_2 coupling. Furthermore, the electrocatalytic urea synthesis process was investigated by operando SR-FTIR (Synchrotron Radiation Fourier Transform Infrared Spectroscopy), and the urea products were detected and quantified via isotope-labeling experiments. As described earlier, the obtained Pd_1Cu_1/TiO_2-400 electrocatalyst can be recognized as tandem catalyst, in which different active sites take charge of different catalytic functions.

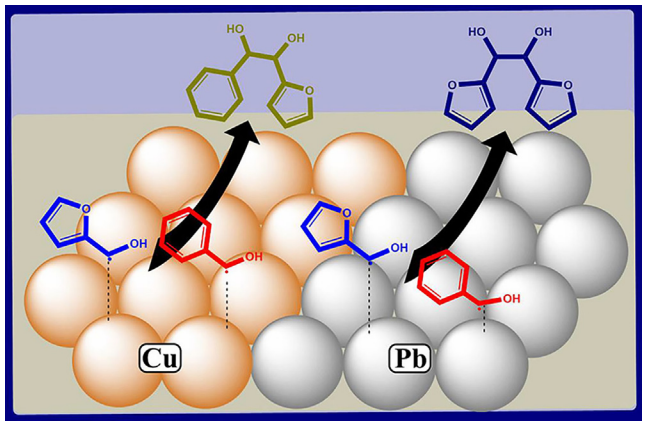

Figure 3. Schematic of the electroreductive coupling system

Reproduced with permission from Anibal et al.[33]

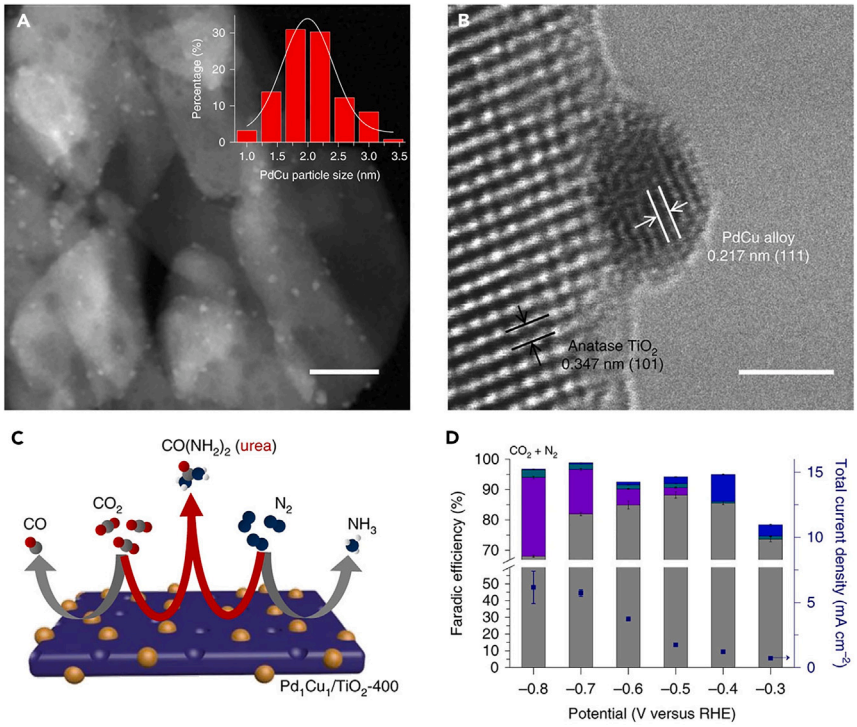

Figure 4. Morphology and electrocatalytic performance of Pd_1Cu_1/TiO_2-400 catalyst

(A and B) (A) TEM image (inset: the distribution of the PdCu nanoparticles, scale bar: 25 nm) and (B) high-resolution TEM image of Pd_1Cu_1/TiO_2-400 (Scale bar: 2 nm).

(C) Schematic diagram for electrocatalytic urea synthesis.

(D) Faradic efficiencies and the total current densities for all products at various potentials. Reproduced with permission from Chen et al.[35]

Thermocatalytic tandem reactions

To date, numerous breakthroughs in tandem reactions have been achieved by globe researchers in terms of different reactants.[36] Among them, one-carbon or single-carbon (C1) molecules transformation has been dominant and received considerable attention. The C1 molecules (including CO_2, CH_4, HCOOH, etc.) are abundant, easily available, and low-costing carbon feedstocks. The transformation of C1 feedstocks into value-added multi-carbon (C_{2+}) compounds is a very meaningful but highly challenging target,[8,37] which has been also discussed in some previous reviews.[38,39]

The homogeneous and heterogeneous thermocatalytic catalysis has played crucial roles in C1 chemistry through carbon–carbon (C–C) bond coupling tandem reactions from CO_2 molecules, resulting in liquid fuel products (e.g., gasoline, diesel, and jet fuel)[40–42] or building-block chemicals (e.g., C_2H_4, C_3H_6, and aromatics).[8,37] However, most of these reactions only operate under harsh conditions, including high temperatures and/or high pressures. Moreover, the selectivity of products, especially the C_{2+} compound, is difficult to control, according to the Anderson-Schulz-Flory (ASF) model.[43] Thus, greener and milder technologies, including photocatalysis and electrocatalysis, have been emerging as promising solution for the activation and selective conversion of C1 molecule into different types of products under ambient conditions.[44–46]

The coupling or addition reactions of aryl molecules into aromatic or biphenyl compound are also attractive types of tandem reaction. In 1901, Ullmann et al. first reported the discovery of the formation of biphenyl compounds by C–C coupling reaction of two aryl halides. The named Ullmann coupling reaction (including C–C, C–N, and C–O coupling),[47] along with Suzuki-Miyaura reaction,[48] etc., is considered as a classical organic reaction pathway in biphenyl synthesis, which has been widely applied in many fields of drugs, semiconductors, liquid crystals, organic conductors, etc. In all cases, these cross-coupling reactions all involved two substrates with complementary functional groups that would be removed before the coupling into aryl products, which are typical tandem reactions. Moreover, Heck-Mirozoki reaction[49] of aryl halides with activated C=C groups and Sonogashira coupling reaction[50] of terminal acetylenes with aryl halides are both typical traditional tandem reactions.

Accordingly, conversion of multiple small molecules into long-chain polymers is developed as an emerging type of tandem reaction.[51,52] In particular, heterogeneous catalytic one-pot synthesis of benzene-fused heterocycles or polyphenyl compounds can be extended as a general approach to aromatic polymers, which are important for optical, fiber, anti-flame, and smart-textile applications.[16,53]

In recent years, the thermocatalysis (or called heterogeneous catalysis) comes out to be a hot issue for development of green-chemistry organic transformations.[54,55] The typical thermocatalysis generally undergoes the process of adsorption of reactant molecules, activation of

Table 2. Thermocatalytic tandem reactions

Reaction	Catalyst	Condition	Reactivity	Year
Conversion of CO_2 into value-added aromatics	NaFe/ZSM-5	H_2/CO_2 = 2, 320°C, 3 MPa	light aromatics account for up to 75% of aromatics and p-xylene selectivity of 72%	2021Wei et al.[56]
	6.25Cu-Fe_2O_3/HZSM-5-c	320°C, 3.0 MPa, $H_2/CO_2/N_2$ = 72/24/4	aromatics selectivity of 57.3%	2020 Song et al.[57]
	ae-ZnO-ZrO_2/H-ZSM-5	H_2/CO_2 = 3/1, 340°C, 40 bar, 10 h	aromatics selectivity of 76%, CO_2 conversion of 16%	2020 Zhou et al.[58]
	Cr_2O_3/H-ZSM-5@S-1	350°C, 3 MPa, H_2/CO_2 = 3 (5.42 vol. % CO), TOS = 6 h	direct synthesis of aromatics with 75.9% selectivity at a single-pass CO_2 conversion of 34.5%	2019Wang et al.[59]
	Cr_2O_3/Zn-ZSM-5@SiO_2.	350°C, 3 MPa (26.5% CO_2, 70.25% H_2 and 3.25% Ar	CO_2 conversion of 22.1%, para-xylene selectivity of 38.7% and aromatics selectivity of 58.4%	2019 Wang et al.[60]
	ZnAlOx&H-ZSM-5	$H_2/CO_2/Ar$ = 3/1/0.2, 3.0 MPa and 593 K	aromatics selectivity of 73.9%	2018 Ni et al.[61]
Convert CO_2 to gasoline-range (C_5–C_{11}) hydrocarbons	Na-Fe_3O_4/HZSM-5	H_2/CO_2 = 3, 320°C, 3 MPa	C_5–C_{11} hydrocarbons selectivity of 78% with CO_2 conversion of 22%	2017 Wei et al.[62]
Conversion CO_2 to lower olefins	$ZnAl_2O_4$/SAPO-34	H_2/CO_2 = 3; p = 3 MPa; T = 643 K; 10 h	C_2-C_4 olefins selectivities reaches 80% (CO conversions of 24%, 673 K) and 87% (CO_2 conversions of 15%, 643 K)	2020 Liu et al.[63]
	Fe/C + K (0.75 wt. %)	320°C, 30 bar, H_2/CO_2 = 3, and 24 000 mL·g-1·h-1, TOS = 50 h.	C_2-C_6 olefin selectivity of 36%	2018 Ramirez et al.[64]
	In-Zr/SAPO-34	400°C, 3.0 MPa, $H_2/CO_2/N_2$ = 73/24/3	$C_2^=$-$C_4^=$ selectivity of 76.40% at 400°C	2017 Gao et al.[65]
	ZnZrO/SAPO	380°C, 2 MPa,	80% selectivity of $C_2^=$–$C_4^=$, 14% C_2–C_4^0, 3% CH_4, and 3% C_{5+}	2017 Li et al.[66]
CO_2 hydrogenation to higher alcohols	4.6K-CMZF	$H_2/CO_2/N_2$ = 72/24/4, 320°C, 5 MPa	selectivity (22.8%, CO-free) and HA STY (69.6 mg g_{cat}^{-1} h^{-1}, 1.47 mol g_{cat}^{-1} h^{-1}) with a C_{2+}OH/ROH fraction of 89.8%	2020 Xu et al.[67]
Synthesis of acetic acid by simultaneous co-activation of CH_4 and CO_2	Cu-K-ZSM-5	500°C in a continuous-flow reactor.	acetic acid yield of 395 mol g_{cat}^{-1} h^{-1} for 10 h.	2017 Rabie et al.[68]
Cycloaddition of CO_2 and SO to yield SC	$B_{0.1}$CN/SBA-15	1 mL SO, 130°C, 3 MPa CO_2, t = 24 h	SO conversions of 97.80%, SC selectivity of 96.8%	2017 Zhu et al.[69]

chemical bonds, formation of intermediates, conversion of intermediates into products, and desorption of final product molecules on catalyst surface. The interaction between molecules/intermediates and catalyst surface is the most decisive issue in thermocatalytic reactions. Although most of C–C, C–N, and C–O coupling reactions were already achieved by traditional thermocatalytic systems, reducing the byproduct and chemical-waste output during organic transformation reactions is also a important goal in the green-chemistry synthesis. Rational design of nano-scale catalysts and one-pot tandem reactions may be potential solutions to achieve these meaningful targets.

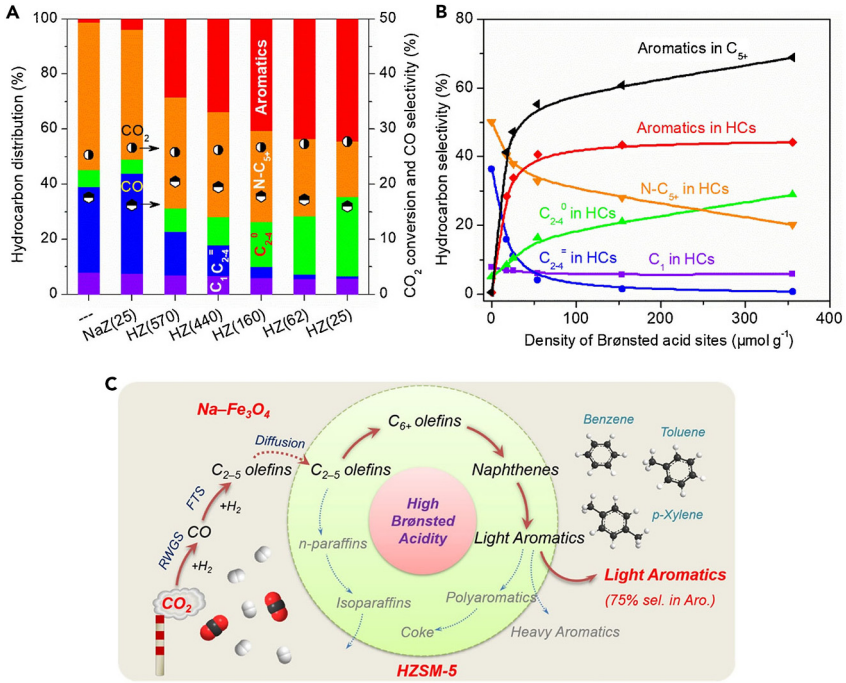

Figure 5. Thermocatalytic performance and reaction path over NaFe/HZSM-5 composite catalysts

(A) Thermocatalytic performance by a series of NaFe/ZSM-5 catalysts.

(B) Relationship between product selectivity and BAS density.

(C) Diagram of light aromatic synthesis via CO_2 hydrogenation over NaFe/HZSM-5 composite catalysts. Reproduced with permission from Wei et al.[56]

Specifically, the thermocatalysis exhibits strong ability in facilitating the tandem chain growth via coupling of CH_x to C_nH_m intermediates, as already discussed in some previous reviews.[5,8] Thus, developing thermocatalysis to operate under lower temperature and pressure occupies an important place in tandem reactions. Some typical examples are listed in Table 2 in the following.

Through combination with metal-oxide catalysts, ZSM-5-based zeolites with variety of active sides and well-designed channel structure have been adopted widely in value-added aromatics production.[56,60,61] Recently, Sun et al. studied a series of composite catalysts integrating Fe-based catalysts with ZSM-5 zeolites to explore the influence of Brønsted acid sites (BASs) on aromatic synthesis and coke formation during CO_2 hydrogenation.[56] As shown in Figure 5A, a moderate acidity is required for the selective synthesis of liquid hydrocarbons (C_{5+}) and aromatics. Moreover, the results in Figure 5B indicate that a relatively high BAS density is favorable for aromatization. Based on previous analysis, the researchers proposed a possible reaction path of light aromatic synthesis from CO_2 hydrogenation over NaFe/HZSM-5 catalyst (Figure 5C). Apparently, the ZSM-5 zeolites exhibited great application potential as a nano-level tandem reactor for light aromatic production.

Organic synthesis by co-activation of smaller molecule feedstocks (like CO_2, CH_4, N_2, etc.) is also a typical tandem reaction.[35,68] In 2017, Park and co-workers reported the formation of acetic acid (CH_3COOH) operated under the continuous-flow microreactor system by the concurrent feed of CH_4 and CO_2 over Cu-loaded M-ZSM-5 (M = Li^+, Na^+, K^+, and Ca^{2+}) catalysts.[68] Their thermocatalytic performance is revealed in Figures 6A and 6B. Based on a series of experimental results, a plausible mechanism is obtained and shown in Figure 6C toward the CH_3COOH formation through co-activation of CH_4 and CO_2 on Cu-K^+−ZSM-5 zeolite. The Cu^0 and M-ZSM-5 contributed to CH_4 and CO_2 activation, respectively, in favor of formation of surface acetate intermediate (−Cu−OOC−CH_3), which can be seen as typical tandem catalyst.

Controlled polymerization of aromatic polymers (including PBO, etc.) could be achieved through tandem reactions.[70] In 2019, Yu and co-workers reported that the controlled polymerization of PBO (Mw = 3.6 kDa) in one-pot reaction is achieved by an AuPd NP system.[16] The 8-nm Au seeding NPs for synthesis of AuPd alloy NPs and as-prepared 8.2 ± 0.4 nm AuPd alloy support on carbon ($Au_{39}Pd_{61}$/C) are shown in Figures 7A and 7B, respectively. Correspondingly, the uniform distributions of Au and Pd of as-prepared $Au_{39}Pd_{61}$/C catalyst were verified by the high-angle annular dark field (HAADF) scanning TEM (STEM) and elemental mapping (Figure 7C). The one-pot reaction is shown in Figure 7D with formic acid as hydrogen source. They proved that the AuPd NP-catalyzed one-pot reaction is a new synthesis path to obtaining highly pure PBO, as chemical purity is essential for the PBO to maintain its thermomechanical stability. The fabricated bimetal NPs catalysts with multi-components corresponding to different bonding-transformation mechanisms are typical tandem catalysts.

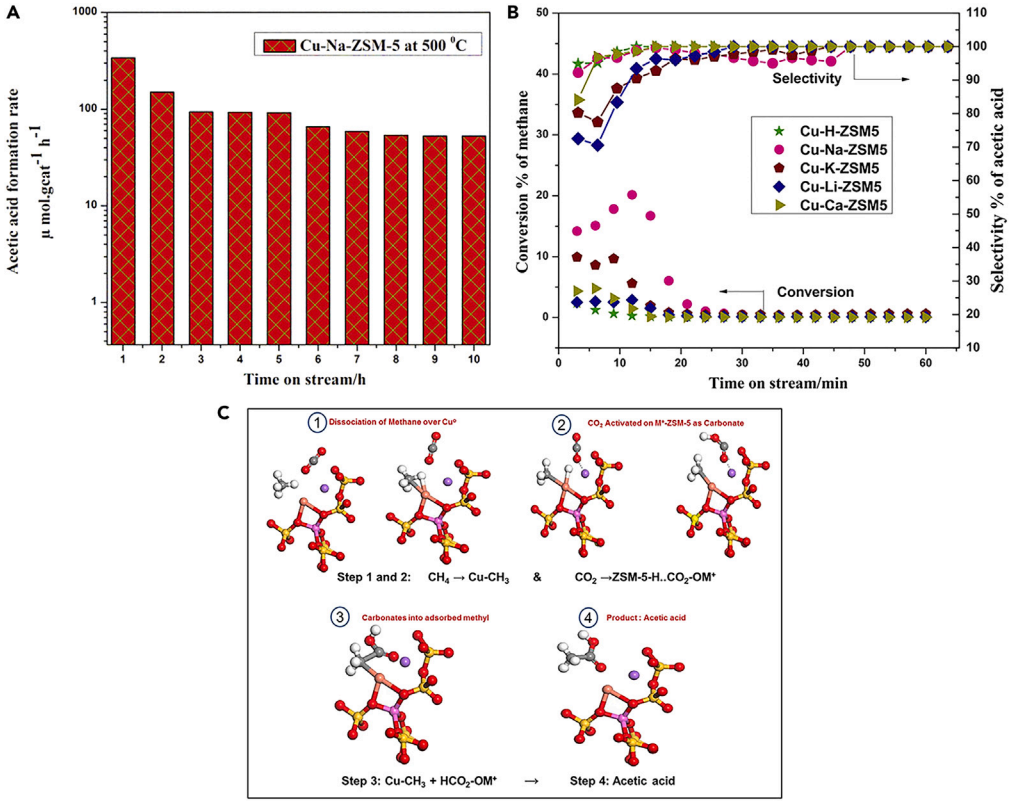

Figure 6. Thermocatalytic performance and reaction path over Cu-K^+−ZSM-5 zeolite

(A) CH_3COOH formation rates for 10 h.

(B) Effect of CH_4/CO_2 flow ratios on the CH_3COOH formation at 500°C.

(C) A proposed mechanism for the co-conversion of CH_4 and CO_2 into CH_3COOH over Cu-*M*-ZSM-5 Zeolite. Reproduced with permission from Rabie et al.[68]

Photocatalytic tandem reactions

Based on semiconductor nanomaterials, the essence of photocatalysis is a process of directly converting solar energy into chemical energy. Besides the representative photocatalysts of titanium dioxide (TiO_2) and metal oxides, even more high-efficient nanomaterials, including bismuth oxyhalides,[71,72] carbonaceous materials,[73,74] metal sulfides,[75] and bio-mimicking photocatalysts,[76] also have been developed and investigated for their photocatalysis properties. However, most of the photogenerated electron and holes in single-phase photocatalyst tend to recombine rapidly due to the strong Coulombic force, resulting in a rather low quantum efficiency.[77] To improve the solar-to-chemical-energy conversion efficiency, diverse effective strategies have been studied to suppress the recombination of photogenerated charges in photocatalysts, including heteroatom doping, metal loading, heterojunction construction,[78,79] etc.

Meanwhile, a growing number of researchers are still making efforts to achieve further breakthrough on improving photocatalytic efficiency and exploiting new application fields. Especially in CO_2 photoconversion, designing tandem reaction systems with multiple active centers or components turned out to be an efficient strategy to tune the CO_2 adsorption modes, preserve CO intermediates or carbon-containing radicals, and coupling processes for multi-carbon products.[38] Some related photocatalytic tandem systems for C–C coupling are listed in the following (Table 3).

Incident light absorption of semiconductors is the first and foremost process in photocatalysis. To take full advantage of solar energy, construction of photocatalysts with multi-components corresponding to different range of sunlight spectrum has attracted increasing attention in recent years.[85,86] In 2022, an oxygen-doped MoS_2@In_2S_3/Bi_2S_3 core-shell dual Z-scheme tandem heterojunctions was constructed by Wang et al.,[87] demonstrating a broad-spectrum response and outstanding photothermal effect, which contributes to the near-field temperature rise and photocatalytic process (Figure 8A). As the ultraviolet visible diffuse reflectance spectra of prepared samples in Figure 8B, Bi_2S_3 mainly absorbed the ultraviolet and visible light regions with low absorption in the infrared light region, while MoS_2 exhibits broad-spectrum light absorption from UV to NIR (near infrared). After integration of MoS_2, In_2S_3, and Bi_2S_3, the absorption peak of composite heterojunction increases obviously, and meanwhile the absorption edge shifts to longer-wavelength region. The fabricated Z-scheme tandem heterojunction composites exhibited a significantly improved photocatalytic H_2 production rate of 973.42 μmol h^{-1} g^{-1}, as well as the degradation efficiency for tetracycline of 99.6% within 90 min (Figure 8C).

Since the light harvesting is essential for photocatalytic reactions, constructing tandem heterojunctions to take charge of different light-spectrum ranges, and meanwhile accelerate charge separation, has been proven to be a promising route to enable full light spectrum-induced reactions,[88,89] which can be defined as tandem catalyst strategy.

With advantage of spatial separated electrons and holes for corresponding redox reaction, the photocatalysis technology has been widely applied in energy conversion and environmental remediation fields in recent years.[90–92] In 2020, Parida et al. fabricated a bimetallic Au/Pd alloy decorated mesoporous silica modified g-C_3N_4 composited photocatalyst for tandem reaction of simultaneous oxidation of phenol and reduction of Cr (VI).[93] This work developed an efficient way to simultaneously degrade two pollutants without any additional chemical reagents, based on the bimetallic co-effect of Au-Pd NPs and Schottky barrier at the interface of Au-Pd alloyed NPs and g-C_3N_4/MCM-41 nanocomposite. The photocatalysts designed in this study with multiple components can simultaneously realize separated oxidation and reduction reactions, which are typical tandem catalysts.

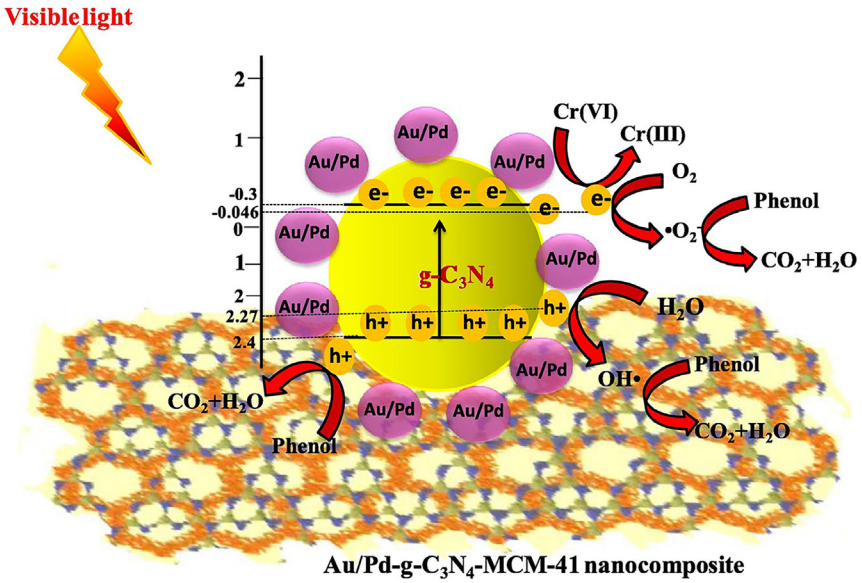

Diagram of photocatalytic tandem reaction process by CNM-AP photocatalyst
Reproduced with permission from Patnaik et al.[93]

TANDEM REACTOR

Tandem reactors refer to a system where two or more reactors, possibly of different types or configurations, are connected in series to facilitate a sequence of reactions or processes. Traditional single reactors, albeit effective for specific processes, often fall short in addressing the multifaceted needs of modern chemical processes. Tandem reactors allow the product from the first reactor to be directly fed into the subsequent reactors, thereby enabling multiple reaction stages to be executed in a streamlined manner. The concept is particularly pertinent when a chemical process involves several intermediate steps or when different reaction conditions are required at different stages.

Constructing tandem reactor with efficient catalysts is more favorable for further practical applications. In 2018, an integrated dual-chamber microreactor coupled with the metal-doped MOFs@COFs was developed by Sun and Kim et al., which was applied in the challenging liquid-gas tandem reactions.[94] The self-designed dual-chamber microreactor was constructed with two circular reaction compartments separated by a gas-permeable PDMS (polydimethylsiloxane) membrane (Figure 9). The tandem reaction was carried out by flowing NH_3BH_3 (AB) solution and ethanol solution containing styrene in the bottom and top chambers, respectively. It can be seen in Figure 9A that the excess of H_2 generated from AB in the bottom chamber can smoothly pass through the PDMS membrane to top chamber for hydrogenation in the continuous-flow device, in which the styrene conversion achieved 94.0% (flow rate: 12.5 μL min^{-1}), as well as a resident time of ≈68 s, significantly superior to the photocatalytic performance in a bulk reactor. With great potential in practical application, tandem reactors would be a hot research issue in the near future.

Producing biofuels from waste oils is highly value added but challenging, which has been investigated by global researchers. Tandem reactor holds great potential to settle the challenging issue. For example, Wang and co-workers developed a bifunctional Ni/Al_2O_3-SiO_2 catalyst to realize a tandem vapor-phase hydrotreating process for waste cooking oils (Figure 10A) through a two-stage fixed bed reactor.[95] Figure 10B indicates a Japanese two-stage fixed bed reactor (RX3050TR). Through the two-stage fixed bed reactor, 83.9 wt % C_5-C_{19} n-alkanes could be obtained from waste cooking oils with a 100% hydrodeoxygenation efficiency in both liquid and gas products.

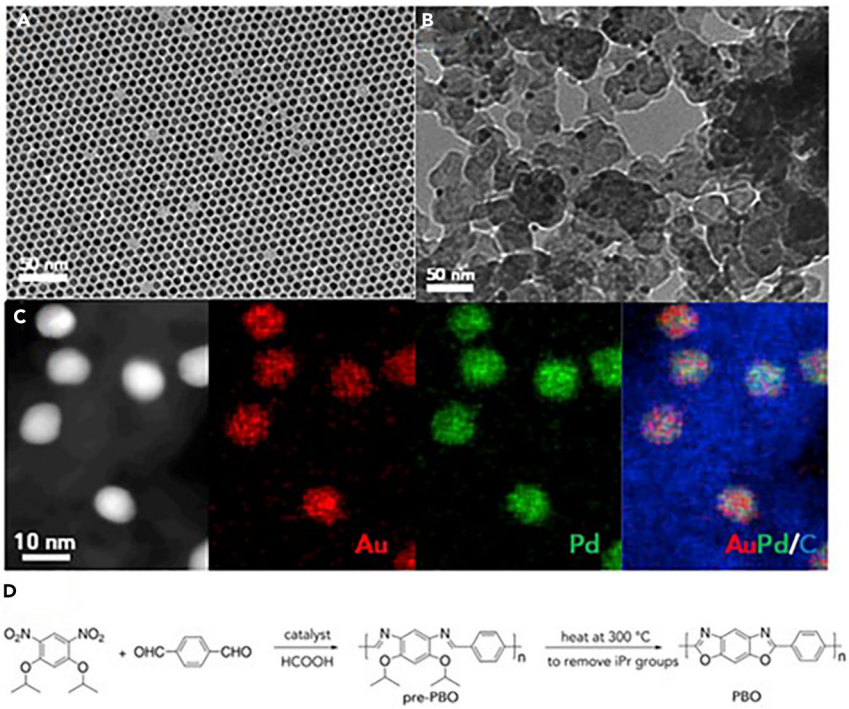

Figure 7. Morphology and reaction path of $Au_{39}Pd_{61}$/C

(A) TEM image of 8-nm Au NPs.

(B and C) (B) TEM image of $Au_{39}Pd_{61}$ NPs deposited on C support, (C) HAADF-STEM image of the $Au_{39}Pd_{61}$/C and elemental mapping of NPs to show Au (red) and Pd (green) distribution within the NPs.

(D) A new synthetic path to synthesize PBO. Reproduced with permission from Yu et al.[16].

Meanwhile, tandem reactor can be also applied to convert CO_2 to multi-carbon product. In 2022, Biswas et al. designed a two-step tandem electrochemical-thermochemical reaction system (Figure 11) for CO_2 conversion to C_3 oxygenates.[96] Specifically, CO_2 was firstly electrochemically reduced to ethylene, CO, and H_2 by Cu catalyst with different oxidation states and hydrophobic gas-diffusion layer, followed by the thermochemical hydroformylation reaction catalyzed by a Rh_1Co_3/MCM-41 to obtain 1-propanol and propanal, achieving a total C_3 oxygenate production rate up to 11.8 μmol min^{-1}.

Continuous-flow system with advantages of flexibility, low cost, efficient operation/product separation, etc., has aroused increasing attentions in recent years.[97] In 2022, the tandem continuous-flow reactors (Figure 12) were developed by Xu et al. to achieve the enzymatic deacidification of rice bran oil (RBO) and simultaneous functional oils production.[98] Through the tandem continuous-flow enzymatic reactors, 91.4% of free fatty acid was removed, and phytosterol ester and diacylglycerol in RBO increased by 9 and 12 times, respectively, along with the significantly enhanced retention rate of γ-oryzanol, in comparison with traditional alkali refining.

Recently, a microfluidic-based autolab with open structures was constructed by *Deng* et al., defined as Put & Play Automated Microplatform (PPAM).[99] Specifically, the microfluidic-based PPAM device (Figure 13A) was composed of two modules arranged around a central control station, in which the "Put" and "Play" take responsibility for catalyst loading/packing and performing/recycling, respectively. The reaction processes for pyridinium chlorochromate (PCC) (upper flow channel) and phase change material (PCM) (lower flow channel) in 3D microchannel models were illustrated in Figures 13B and 13C, indicating that the catalytic activity could be easily modulated by different channel sizes of reactor. The interesting phenomena in this work would contribute to the understanding and research of heterogeneous catalysis through microfluidic-based tandem reactors.

TANDEM FIELDS (INCLUDING PHOTOELECTROCATALYSIS [PEC], PHOTOTHERMAL CATALYSIS, ETC.)

In comparison, the photocatalysis and electrocatalysis operated under ambient conditions are rather economy-saving, eco-friendly, and low-cost strategies in tandem reactions. Relatively, the thermocatalysis reveals higher selectivity toward multi-carbon (C_{2+}) hydrocarbons, due to the high-power input (e.g., high temperature and pressure) to overcome the energy barrier. Thus, combination of advantages from different driven energy field, including light, electricity, and heat, should be potential solutions to settle the shortcoming of traditional catalysis. The synergistic effect of multi-physics fields for catalytic reactions can be defined as tandem fields or tandem catalytic fields.

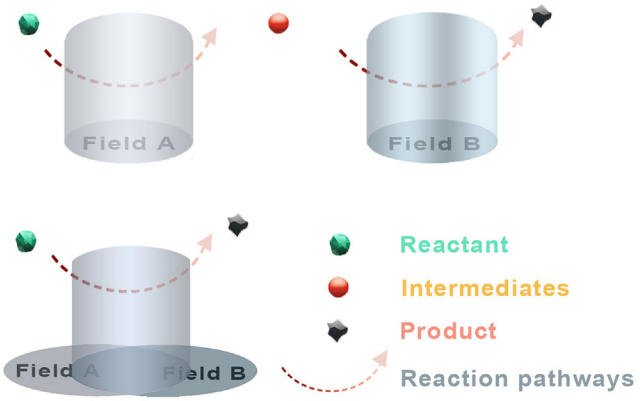

Diagram of different synergies between tandem fields

PEC has been proved to be an efficient strategy in water splitting, CO_2 reduction, N_2 reduction reaction, etc.[90,100] Recently, Jing et al. reported the fabrication of a series of three-dimensional C/N-doped heterojunctions of Zn_x:Co_y@Cu (Figure 14A), which served as photocathodes in PEC reduction of CO_2 to obtain paraffin product (Figure 14B).[14] The actual optical photographs shown in Figure 15C indicate the photoelectrodes ($BiVO_4$ photoanode and Zn_x:Co_y@Cu photocathode) and the paraffin product. In the constructed PEC cell (Figure 14C), the researchers demonstrated that the C/N-doped Zn_x:Co_y@Cu heterojunctions photocathode mimics the Calvin cycle of plants, realizing multiple C–C couplings to generate the paraffin product. The photogenerated electrons and holes from Zn_x:Co_y photocatalyst would be driven by external electric field to suppress the charge recombination, which subsequently participate in paraffin production and O_2 evolution, respectively. The PEC is a reaction process driven by tandem field of light and electricity.

Table 3. Photocatalytic tandem reactions

Reaction	Catalyst	Condition	Reactivity	Year
Conversion of CO_2 into C_2H_5OH	TiO_2	UV-enhanced Xe light; CO_2-saturated 0.1 M $NaHCO_3$	C_2H_5OH yield rate of 6.16 mmol g^{-1} h^{-1}	2020 Jiang et al.[80]
CO_2 reduction to yield C_1 (methane) and C_2 (ethane)	plasmonic Au NP	isopropyl alcohol (IPA, 10% v/v), 300 W Xe lamp (ca. 300 mW cm^{-2}, 3.14 cm^2 in area) with 400 nm filter	CH_4 TONs of ~6.8 NP^{-1} and C_2H_6 TONs of ~5.6 NP^{-1} after 10 h illumination	2018 Yu et al.[46]
CO_2 reduction pairing with selective oxidation of BA	CTAB-$ZnIn_2S_4$	5 mL CH_3-CN containing 5 mL BA; 300 W Xe arc lamp with a 420 nm cut-off filter, 0.8 W cm^2	hydrobenzoin and benzoin selectivity of 93%	2020 Yuan et al.[81]
Selective photoreduction of nitroaromatic compounds to synthesize azo- and azoxyaromatic dyes	g-C_3N_4	0.01 M KOH, room temperature	azoxyaromatics selectivity of 95% (450 nm, 12 h); azoarmomatics selectivity of 94% (410 nm, 5 h)	2018 Dai et al.[82]
C–C coupling of benzyl alcohol (BA) into hydrobenzoin (HB)	2.5%CdS/SiO_2	10 mL of CH_3CN containing 25 μL (0.24 mmol) of BA. 300 W Xe lamp (300 mW cm^{-2})	BA conversion of 85.4%.an HB production rate of 17.0 mmol g_{CdS}^{-1} h^{-1} can be obtained with a yield of 84.6% (12 h reaction time)	2020 Qi et al.[83]
Pinacol C-C coupling of benzaldehyde to hydrobenzoin	$ZnIn_2S_4$	room temperature; 9 mL of CH_3CN, 1 mL of H_2O, 1 mL of TEA, blue LED, 4 h	C-C coupling products (including hydrobenzoin) selectivity of 98%	2020 Zhang et al.[84]

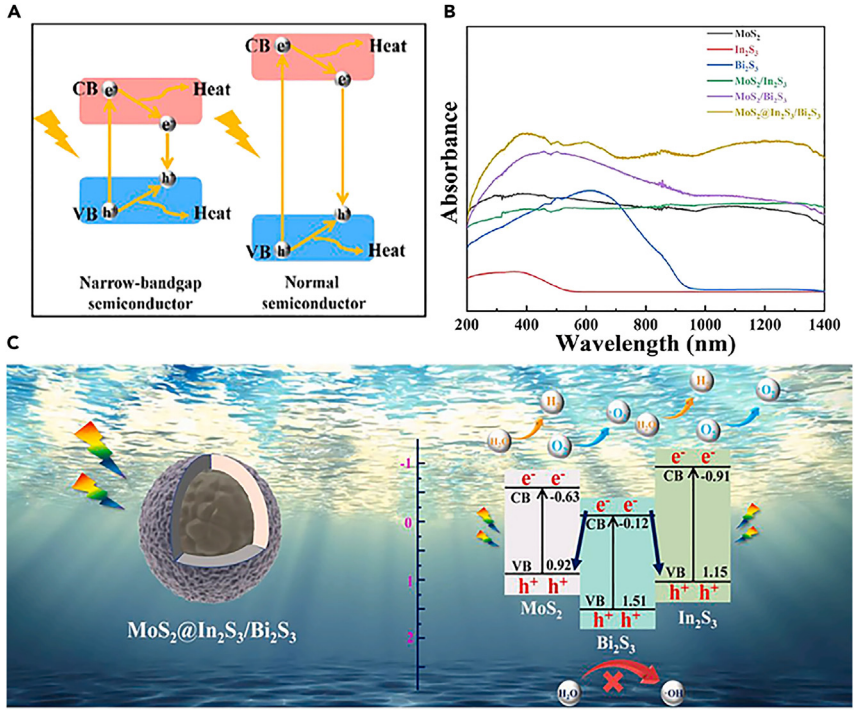

Figure 8. Core-shell dual Z-scheme tandem heterojunctions

(A) UV-vis DRS spectra of prepared photocatalysts.

(B) Comparison of electron-hole generation and recombination in a narrow-bandgap and normal semiconductor.

(C) The proposed photocatalytic mechanism of MoS_2@In2S3/Bi_2S_3 tandem heterojunctions. Reproduced with permission from Wang et al.[87]

Tandem fields of photo- and thermocatalysis are more favorable for high catalytic performance and selectivity toward specific chemical-bonds activation.[101,102] In 2020, Li and co-workers reported the ultrathin porous g-C_3N_4 nanosheets modified with AuCu alloy NPs (Figure 16A) for photothermal catalytic CO_2 reduction to ethanol (C_2).[103] Among different catalytic processes, the highest ethanol (C_2) selectivity

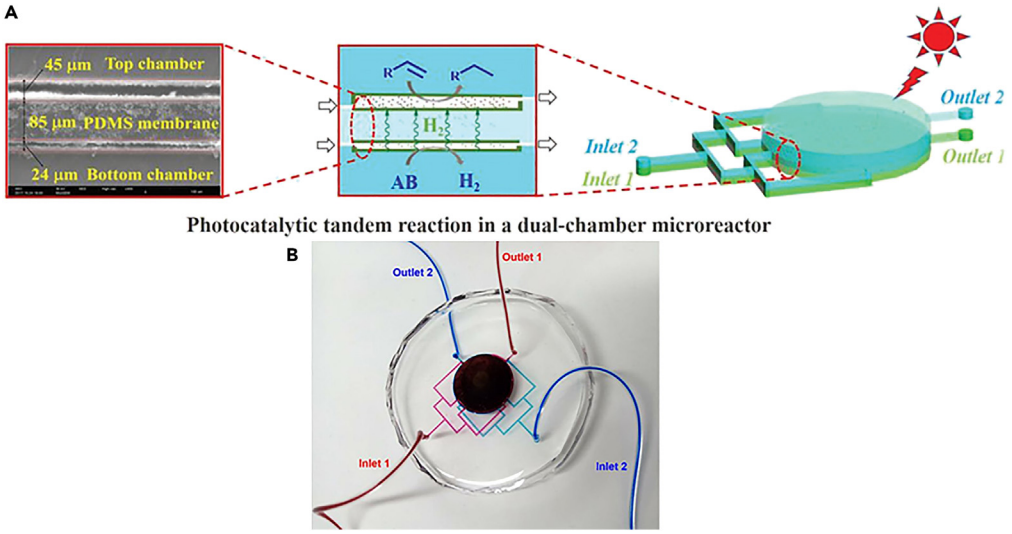

Figure 9. The dual-chamber microreactor

(A) Diagram of photocatalytic tandem microreactor.

(B) Photograph of the constructed dual-chamber microreactor. Reproduced with permission from Sun et al.[94]

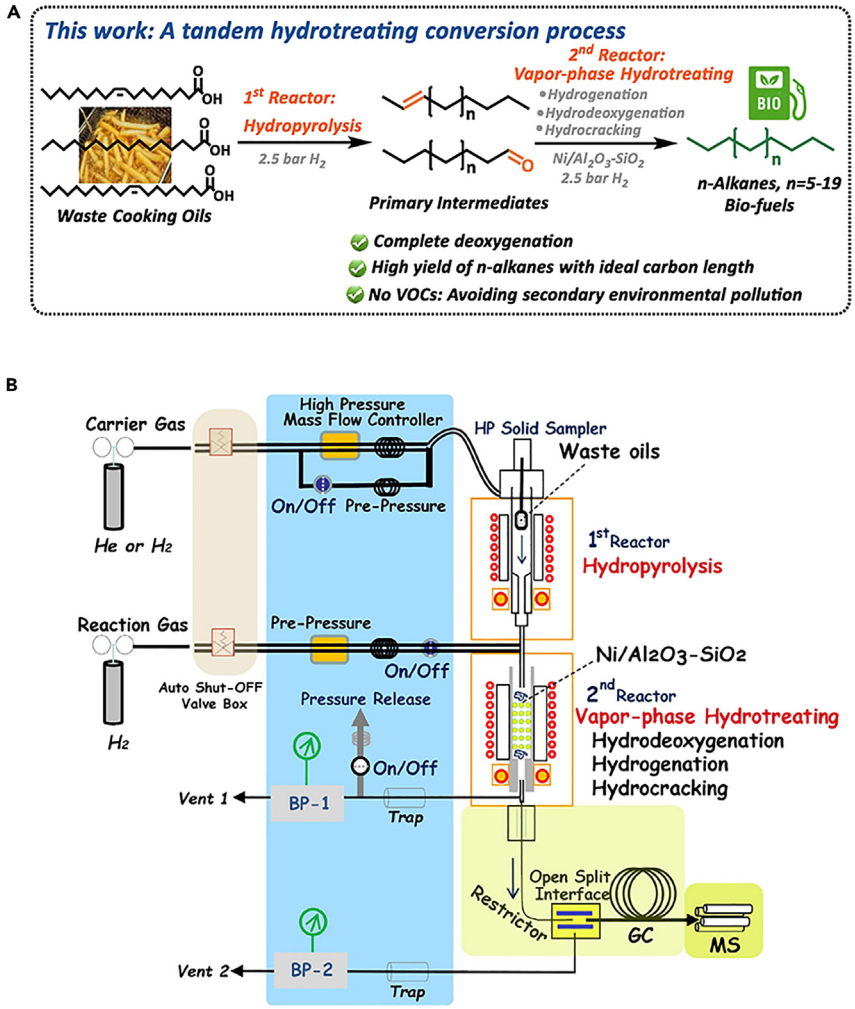

Figure 10. Tandem reactor for waste oils conversion

(A) Tandem hydrotreating process for waste oil.

(B) Two-stage pressurized fixed bed reactor. Reproduced with permission from Wang et al.[95].

of the AuCu/g-C_3N_4 reaches 93% under photothermal synergistic catalysis (Figure 16B). As revealed in Figure 16C, the ethanol yield raised to top, when the temperature increased up to 120°C.

Conclusion

Summary

To date, tandem processes continue to present both challenging and promising directions. This paper provides a systematic organization and description of the utilization of catalysts, reactors, and energy fields as efficient and eco-friendly carriers for tandem reactions, employing various energy fields which include electric, thermal, and photothermal energy, and shows the research progress of tandem reactions in recent years. In the field of nanomaterial design, this review highlights the effects of rational design and the integration of diverse energy fields on the conversion of functional groups and the formation and breakage of chemical bonds during chemical reactions. Additionally, controlling intermediates improves chemical yields, while enabling the realization of chemical pathways that are challenging to conduct under typical conditions.

Future perspectives

In summary, this review explores variety of tandem processes, including tandem catalyst, tandem reactor, and tandem field, all driven by well-designed nanocatalysts, demonstrating immense potential in applications such as CO_2 upgrading, biphenyl generation, and polymer synthesis. Hence, we emphasize the emerging trend of the tandem field, which combines the advantages of electro-, thermo- and photocatalysis.

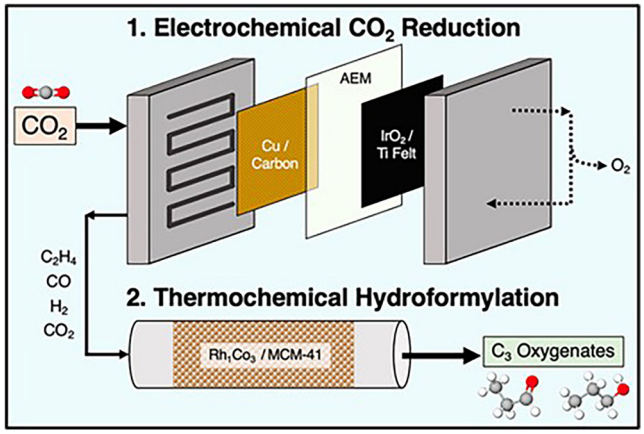

Figure 11. Diagram of tandem electrochemical-thermochemical reactors
Reproduced with permission from Biswas et al.[96]

This convergence is projected to set new benchmarks in nanomaterial design and catalysis, paving the way for high-performance, energy-efficient, environmental-friendly tandem reactions. Specifically, the key to achieving these outcomes is the optimization of nanocatalysts preparation, leveraging appropriate functional materials to settle pivotal factors in catalytic processes, and aiming toward cost-effectiveness, stability, and scalability. These strategies are essential for enhancing the activity, yield, and stability of the desired tandem reactions.

Additionally, to provide a comprehensive understanding of the tandem reaction pathway, it is imperative to focus on mechanism study of catalyst, considering aspects like defects, facets, and vacancies. This can be achieved through control experiments and advanced theoretical simulation, including density functional theory (DFT) and first principal theory.

Limitations of the study

As is typical in scientific research, our study also has certain limitations. Our investigation primarily focuses on the role of catalysts, reactors, and fields in tandem reactions, aiming to provide insights into the macroscopic perspective of interactive and mutually reinforcing factors. However, there are additional aspects that warrant further investigation. For instance, the activity and stability of catalysts are crucial factors that can impact the overall performance of tandem reactions. Further research is needed to address the challenges associated with catalyst activity, such as catalyst deactivation or selectivity loss, thus obtaining high-efficiency and stable catalysts for tandem reactions. Additionally, the potential issue of reactor blockage and its impact on reaction efficiency requires more in-depth exploration.

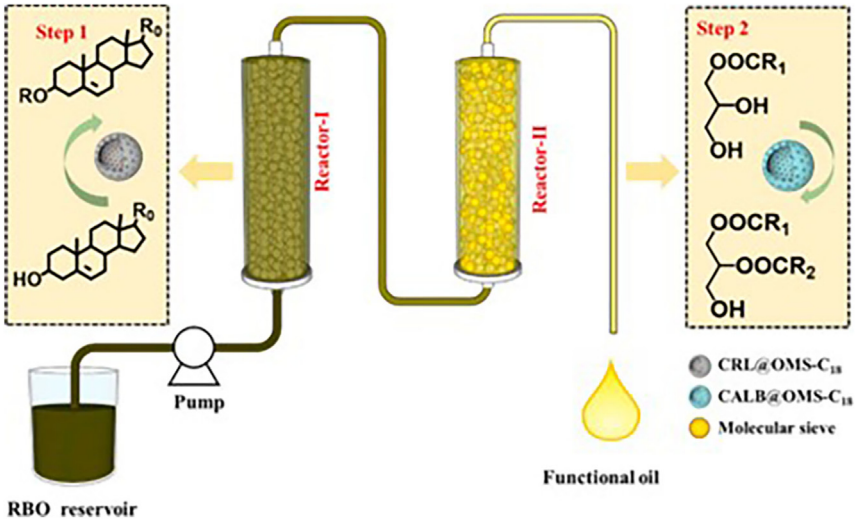

Figure 12. Tandem continuous-flow enzymatic reactors
Reproduced with permission from Xu et al.[98]

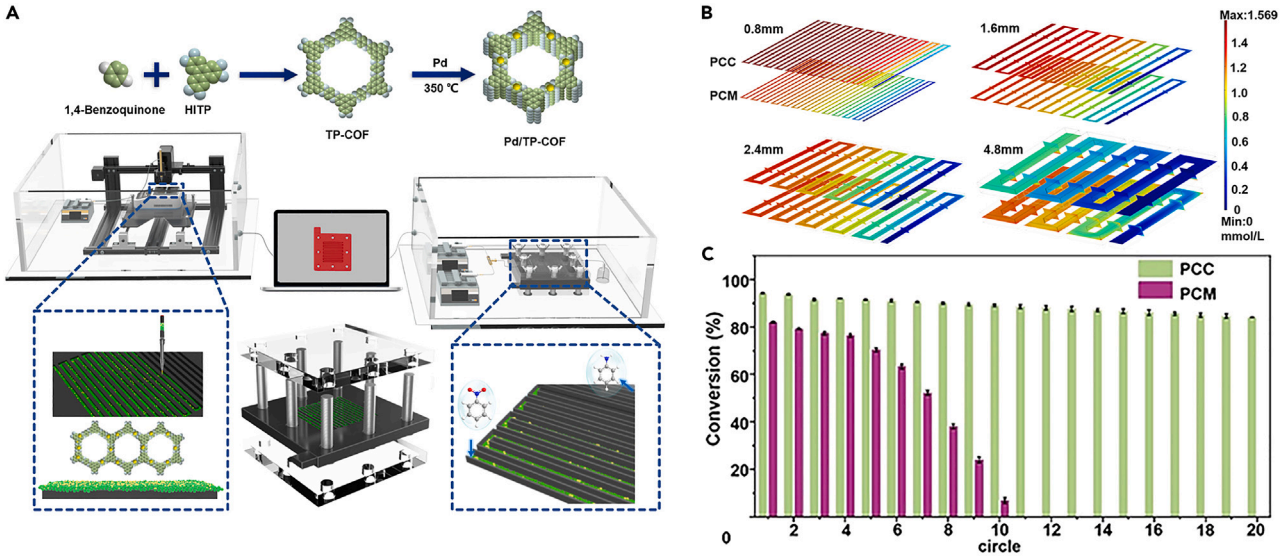

Figure 13. Microfluidic-based autolab PPAM model

(A) PPAM model display.

(B) Aniline distribution in 3D microchannel models with PCC and PCM in 1 min.

(C) Cycle stability test of the aniline production. Reproduced with permission from Deng et al.[99]

ACKNOWLEDGMENTS

W.W. and J.H. contributed equally to this work. This work was supported by the National Natural Science Foundation of China (52003121, 2220081350) and the China Postdoctoral Science Foundation (2020M671497, 2020T130300).

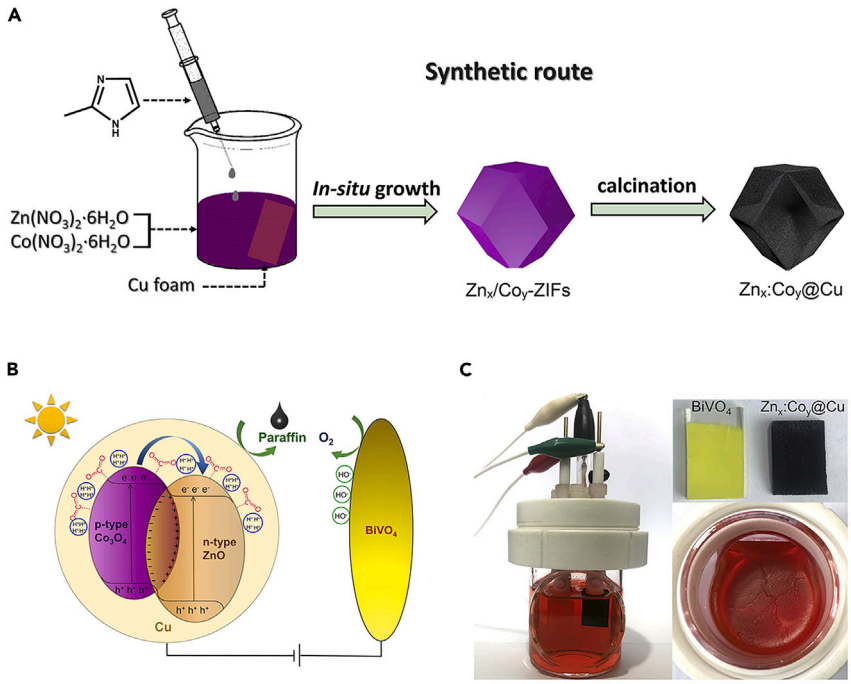

Figure 14. Catalyst preparation and tandem PEC reaction diagram of Zn_x:Co_y@Cu photocathode

(A and B) (A) Preparation route of Zn_x:Co_y@Cu photocathode and (B) the artificial photosynthesis of paraffin.

(C) Optical photographs of PEC cell, photoelectrodes, and paraffin product on electrolyte. Reproduced with permission from Wang et al.[14]

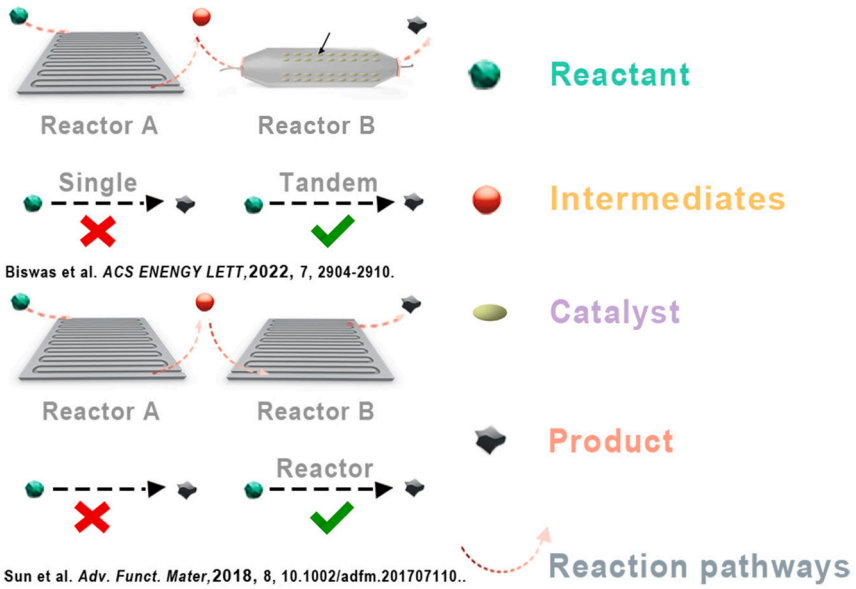

Figure 15. Diagram of the advantages of tandem reactors

AUTHOR CONTRIBUTIONS

Conceptualization, W.W. and C.Y., writing – original draft, W.W. and J.H.; visualization, J.H.; supervision, X.C. and C.Y.; revision, C.Y. and J.D.

DECLARATION OF INTERESTS

The authors declare no competing interests.

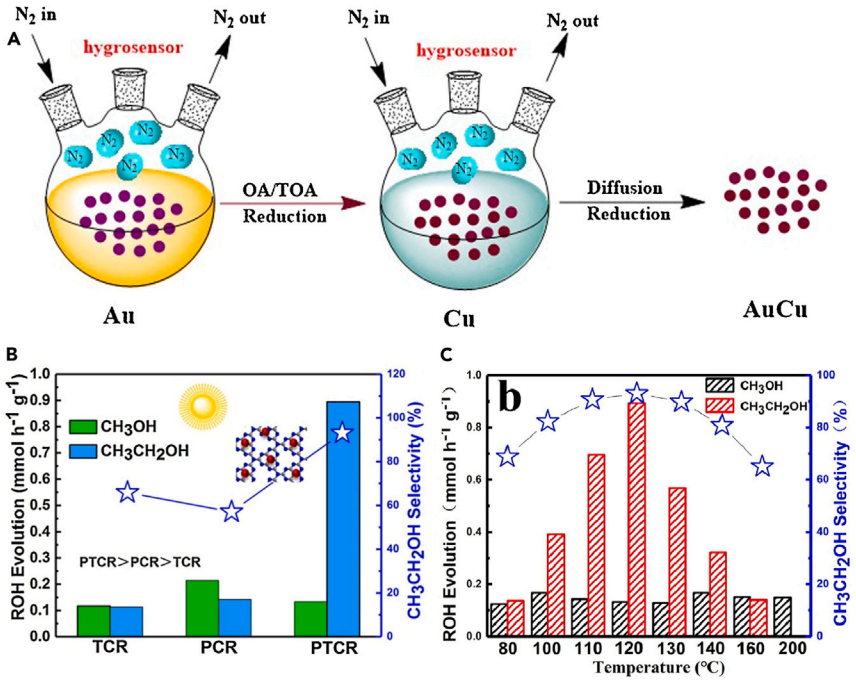

Figure 16. Alloy formation and tandem photothermocatalytic performance of AuCu/g-C_3N_4 nanocomposites

(A) Diagram of AuCu alloy formation process.

(B and C) (B) Comparison of TCR, PCR, and PTCR performances over AuCu/g-C_3N_4 nanocomposite, (C) product yields of ROHs over AuCu on different temperatures. Reproduced with permission from Li et al.[103]

REFERENCES

1. Chen, F., Jiang, X., Zhang, L., Lang, R., and Qiao, B. (2018). Single-atom catalysis: Bridging the homo- and heterogeneous catalysis. Chin. J. Catal. *39*, 893–898.
2. Huang, Y.-B., Liang, J., Wang, X.-S., and Cao, R. (2017). Multifunctional metal–organic framework catalysts: synergistic catalysis and tandem reactions. Chem. Soc. Rev. *46*, 126–157.
3. Fogg, D.E., and dos Santos, E.N. (2004). Tandem catalysis: a taxonomy and illustrative review. Coord. Chem. Rev. *248*, 2365–2379.
4. Tang, C., Zheng, Y., Jaroniec, M., and Qiao, S.Z. (2021). Electrocatalytic Refinery for Sustainable Production of Fuels and Chemicals. Angew. Chem. Int. Ed. *60*, 19572–19590.
5. Lohr, T.L., and Marks, T.J. (2015). Orthogonal tandem catalysis. Nat. Chem. *7*, 477–482.
6. Mishra, S., and Aponick, A. (2019). Lactone Synthesis by Enantioselective Orthogonal Tandem Catalysis. Angew. Chem. Int. Ed. *58*, 9485–9490.
7. Cho, H.J., and Xu, B. (2020). Enabling Selective Tandem Reactions via Catalyst Architecture Engineering. Trends Chem. *2*, 929–941.
8. Ma, Z., and Porosoff, M.D. (2019). Development of Tandem Catalysts for CO_2 Hydrogenation to Olefins. ACS Catal. *9*, 2639–2656.
9. Sun, K., Wang, X., Li, C., Wang, H., and Li, L. (2020). Recent advances in tandem selenocyclization and tellurocyclization with alkenes and alkynes. Org. Chem. Front. *7*, 3100–3119.
10. Guo, Q., Wang, Y., Han, J., Zhang, J., and Wang, F. (2022). Interfacial Tandem Catalysis for Ethylene Carbonylation and C–C Coupling to 3-Pentanone on Rh/Ceria. ACS Catal. *12*, 3286–3290.
11. Xiao, J., Cheng, K., Xie, X., Wang, M., Xing, S., Liu, Y., Hartman, T., Fu, D., Bossers, K., van Huis, M.A., et al. (2022). Tandem catalysis with double-shelled hollow spheres. Nat. Mater. *21*, 572–579.
12. Patra, S., and Maity, N. (2021). Recent advances in (hetero)dimetallic systems towards tandem catalysis. Coord. Chem. Rev. *434*, 213803.
13. Chen, C., Li, Y., Yu, S., Louisia, S., Jin, J., Li, M., Ross, M.B., and Yang, P. (2020). Cu-Ag Tandem Catalysts for High-Rate CO_2 Electrolysis toward Multicarbons. Joule *4*, 1688–1699.
14. Wang, J., Guan, Y., Yu, X., Cao, Y., Chen, J., Wang, Y., Hu, B., and Jing, H. (2020). Photoelectrocatalytic Reduction of CO_2 to Paraffin Using p-n Heterojunctions. iSci *23*, 100768.
15. Fang, D., Yang, L., Hu, W., Feng, Y., Tu, Y., Geng, Y., Shi, H., Shao, P., Luo, X., Hong, M., and Liu, T. (2021). Tandem type PRBs-like technology implanted with targeted functional materials for efficient resourceful treatment of heavy metal ions from mining wastewater. Chem. Eng. J. *420*, 130506.
16. Yu, C., Guo, X., Yin, Z., Zhao, Z., Li, X., Robinson, J., Muzzio, M., Castilho, C.J., Shen, M., Yuan, Y., et al. (2019). Highly Efficient AuPd Catalyst for Synthesizing Polybenzoxazole with Controlled Polymerization. Matter *1*, 1631–1643.
17. Yu, C., Guo, X., Xi, Z., Muzzio, M., Yin, Z., Shen, B., Li, J., Seto, C.T., and Sun, S. (2017). AgPd Nanoparticles Deposited on $WO_{2.72}$ Nanorods as an Efficient Catalyst for One-Pot Conversion of Nitrophenol/Nitroacetophenone into Benzoxazole/Quinazoline. J. Am. Chem. Soc. *139*, 5712–5715.
18. Huang, H., Denard, C.A., Alamillo, R., Crisci, A.J., Miao, Y., Dumesic, J.A., Scott, S.L., and Zhao, H. (2014). Tandem Catalytic Conversion of Glucose to 5-Hydroxymethylfurfural with an Immobilized Enzyme and a Solid Acid. ACS Catal. *4*, 2165–2168.
19. Climent, M.J., Corma, A., Iborra, S., and Sabater, M.J. (2014). Heterogeneous Catalysis for Tandem Reactions. ACS Catal. *4*, 870–891.
20. Liu, Z., He, J.H., Zhang, M., Shi, Z.J., Tang, H., Zhou, X.Y., Tian, J.J., and Wang, X.C. (2022). Borane-Catalyzed C3-Alkylation of Pyridines with Imines, Aldehydes, or Ketones as Electrophiles. J. Am. Chem. Soc. *144*, 4810–4818.
21. Ma, W., Xie, S., Liu, T., Fan, Q., Ye, J., Sun, F., Jiang, Z., Zhang, Q., Cheng, J., and Wang, Y. (2020). Electrocatalytic reduction of CO_2 to ethylene and ethanol through hydrogen-assisted C–C coupling over fluorine-modified copper. Nat. Catal. *3*, 478–487.
22. Guo, C., Ran, J., Vasileff, A., and Qiao, S.-Z. (2018). Rational design of electrocatalysts and photo(electro)catalysts for nitrogen reduction to ammonia (NH_3) under ambient conditions. Energy Environ. Sci. *11*, 45–56.
23. Jin, H., Guo, C., Liu, X., Liu, J., Vasileff, A., Jiao, Y., Zheng, Y., and Qiao, S.-Z. (2018). Emerging two-dimensional nanomaterials for electrocatalysis. Chem. Rev. *118*, 6337–6408.
24. Hou, J., Wu, Y., Zhang, B., Cao, S., Li, Z., and Sun, L. (2019). Rational design of nanoarray architectures for electrocatalytic water splitting. Adv. Funct. Mater. *29*, 1808367.
25. Zhang, T., Li, Z., Zhang, J., and Wu, J. (2020). Enhance CO_2-to-C^{2+} products yield through spatial management of CO transport in Cu/ZnO tandem electrodes. J. Catal. *387*, 163–169.
26. Zhang, B., Zhang, J., Hua, M., Wan, Q., Su, Z., Tan, X., Liu, L., Zhang, F., Chen, G., Tan, D., et al. (2020). Highly Electrocatalytic Ethylene Production from CO_2 on Nanodefective Cu Nanosheets. J. Am. Chem. Soc. *142*, 13606–13613.
27. Kim, C., Weng, L.-C., and Bell, A.T. (2020). Impact of Pulsed Electrochemical Reduction of CO_2 on the Formation of C^{2+} Products over Cu. ACS Catal. *10*, 12403–12413.
28. Zhao, K., Nie, X., Wang, H., Chen, S., Quan, X., Yu, H., Choi, W., Zhang, G., Kim, B., and Chen, J.G. (2020). Selective electroreduction of CO_2 to acetone by single copper atoms anchored on N-doped porous carbon. Nat. Commun. *11*, 2455.
29. Rahaman, M., Kiran, K., Montiel, I.Z., Grozovski, V., Dutta, A., and Broekmann, P. (2020). Selective n-propanol formation from CO_2 over degradation-resistant activated PdCu alloy foam electrocatalysts. Green Chem. *22*, 6497–6509.
30. Kim, Y., Park, S., Shin, S.-J., Choi, W., Min, B.K., Kim, H., Kim, W., and Hwang, Y.J. (2020). Time-resolved observation of C–C coupling intermediates on Cu electrodes for selective electrochemical CO_2 reduction. Energy Environ. Sci. *13*, 4301–4311.
31. Han, J., Long, C., Zhang, J., Hou, K., Yuan, Y., Wang, D., Zhang, X., Qiu, X., Zhu, Y., Zhang, Y., et al. (2020). A reconstructed porous copper surface promotes selectivity and efficiency toward C2 products by electrocatalytic CO_2 reduction. Chem. Sci. *11*, 10698–10704.
32. Loiudice, A., Lobaccaro, P., Kamali, E.A., Thao, T., Huang, B.H., Ager, J.W., and Buonsanti, R. (2016). Tailoring Copper Nanocrystals towards C2 Products in Electrochemical CO_2 Reduction. Angew. Chem., Int. Ed. *55*, 5789–5792.
33. Anibal, J., and Xu, B. (2020). Electroreductive C–C Coupling of Furfural and Benzaldehyde on Cu and Pb Surfaces. ACS Catal. *10*, 11643–11653.
34. Zhang, T., Bui, J.C., Li, Z., Bell, A.T., Weber, A.Z., and Wu, J. (2022). Highly selective and productive reduction of carbon dioxide to multicarbon products via in situ CO management using segmented tandem electrodes. Nat. Catal. *5*, 202–211.
35. Chen, C., Zhu, X., Wen, X., Zhou, Y., Zhou, L., Li, H., Tao, L., Li, Q., Du, S., Liu, T., et al. (2020). Coupling N_2 and CO_2 in H_2O to synthesize urea under ambient conditions. Nat. Chem. *12*, 717–724.
36. Wolfs, J., Nickisch, R., Wanner, L., and Meier, M.A.R. (2021). Sustainable One-Pot Cellulose Dissolution and Derivatization via a Tandem Reaction in the DMSO/DBU/CO_2 Switchable Solvent System. J. Am. Chem. Soc. *143*, 18693–18702.
37. Gomez, E., Nie, X., Lee, J.H., Xie, Z., and Chen, J.G. (2019). Tandem Reactions of CO_2 Reduction and Ethane Aromatization. J. Am. Chem. Soc. *141*, 17771–17782.
38. Xie, S., Ma, W., Wu, X., Zhang, H., Zhang, Q., Wang, Y., and Wang, Y. (2021). Photocatalytic and electrocatalytic transformations of C1 molecules involving C–C coupling. Energy Environ. Sci. *14*, 37–89.
39. Zhang, Q., Yu, J., and Corma, A. (2020). Applications of Zeolites to C1 Chemistry: Recent Advances, Challenges, and Opportunities. Adv. Mater. *32*, e2002927.
40. Wei, J., Ge, Q., Yao, R., Wen, Z., Fang, C., Guo, L., Xu, H., and Sun, J. (2017). Directly converting CO_2 into a gasoline fuel. Nat. Commun. *8*, 15174.
41. Li, J., He, Y., Tan, L., Zhang, P., Peng, X., Oruganti, A., Yang, G., Abe, H., Wang, Y., and Tsubaki, N. (2018). Integrated tuneable synthesis of liquid fuels via Fischer–Tropsch technology. Nat. Catal. *1*, 787–793.
42. Gao, X., Atchimarungsri, T., Ma, Q., Zhao, T.-S., and Tsubaki, N. (2020). Realizing efficient carbon dioxide hydrogenation to liquid hydrocarbons by tandem catalysis design. J. Energy Chem. *2*, 100038.
43. Puskas, I., and Hurlbut, R.S. (2003). Comments about the causes of deviations from the Anderson-Schulz-Flory distribution of the Fischer-Tropsch reaction products. Catal. Today *84*, 99–109.
44. Xie, S., Ma, W., Wu, X., Zhang, H., Zhang, Q., Wang, Y., and Wang, Y. (2021). Photocatalytic and electrocatalytic transformations of C1 molecules involving C—C coupling. Energy Environ. Sci. *14*, 37–89.
45. Yin, Z., Yu, C., Zhao, Z., Guo, X., Shen, M., Li, N., Muzzio, M., Li, J., Liu, H., Lin, H., et al. (2019). Cu_3N Nanocubes for Selective

Electrochemical Reduction of CO_2 to Ethylene. Nano Lett. *19*, 8658–8663.
46. Yu, S., Wilson, A.J., Heo, J., and Jain, P.K. (2018). Plasmonic Control of Multi-Electron Transfer and C-C Coupling in Visible-Light-Driven CO_2 Reduction on Au Nanoparticles. Nano Lett. *18*, 2189–2194.
47. Ullmann, F., and Bielecki, J. (1901). Ueber synthesen in der biphenylreihe. Ber. Dtsch. Chem. Ges. *34*, 2174–2185.
48. Miyaura, N., and Suzuki, A. (1995). Palladium-catalyzed cross-coupling reactions of organoboron compounds. Chem. Rev. *95*, 2457–2483.
49. Cabri, W., and Candiani, I. (1995). Recent developments and new perspectives in the Heck reaction. Acc. Chem. Res. *28*, 2–7.
50. Chinchilla, R., and Nájera, C. (2011). Recent advances in Sonogashira reactions. Chem. Soc. Rev. *40*, 5084–5121.
51. Shen, R., Zhu, W., Yan, X., Li, T., Liu, Y., Li, Y., Dai, S., and Gu, Z.G. (2019). A porphyrin porous organic polymer with bicatalytic sites for highly efficient one-pot tandem catalysis. Chem. Commun. (Camb) *55*, 822–825.
52. Felpin, F.X., and Fouquet, E. (2008). Heterogeneous multifunctional catalysts for tandem processes: an approach toward sustainability. ChemSusChem *1*, 718–724.
53. Yu, C., Guo, X., Shen, B., Xi, Z., Li, Q., Yin, Z., Liu, H., Muzzio, M., Shen, M., Li, J., et al. (2018). One-pot formic acid dehydrogenation and synthesis of benzene-fused heterocycles over reusable AgPd/$WO_{2.72}$ nanocatalyst. J. Mater. Chem. A *6*, 23766–23772.
54. Hooshmand, S.E., Heidari, B., Sedghi, R., and Varma, R.S. (2019). Recent advances in the Suzuki–Miyaura cross-coupling reaction using efficient catalysts in eco-friendly media. Green Chem. *21*, 381–405.
55. Norouzi, N., Das, M.K., Richard, A.J., Ibrahim, A.A., El-Kaderi, H.M., and El-Shall, M.S. (2020). Heterogeneous catalysis by ultra-small bimetallic nanoparticles surpassing homogeneous catalysis for carbon-carbon bond forming reactions. Nanoscale *12*, 19191–19202.
56. Wei, J., Yao, R., Ge, Q., Xu, D., Fang, C., Zhang, J., Xu, H., and Sun, J. (2021). Precisely regulating Brønsted acid sites to promote the synthesis of light aromatics via CO_2 hydrogenation. Appl. Catal., B *283*, 119648.
57. Song, G., Li, M., Yan, P., Nawaz, M.A., and Liu, D. (2020). High Conversion to Aromatics via CO_2-FT over a CO-Reduced Cu-Fe_2O_3 Catalyst Integrated with HZSM-5. ACS Catal. *10*, 11268–11279.
58. Zhou, C., Shi, J., Zhou, W., Cheng, K., Zhang, Q., Kang, J., and Wang, Y. (2019). Highly Active ZnO-ZrO_2 Aerogels Integrated with H-ZSM-5 for Aromatics Synthesis from Carbon Dioxide. ACS Catal. *10*, 302–310.
59. Wang, Y., Tan, L., Tan, M., Zhang, P., Fang, Y., Yoneyama, Y., Yang, G., and Tsubaki, N. (2018). Rationally Designing Bifunctional Catalysts as an Efficient Strategy To Boost CO_2 Hydrogenation Producing Value-Added Aromatics. ACS Catal. *9*, 895–901.
60. Wang, Y., Gao, W., Kazumi, S., Li, H., Yang, G., and Tsubaki, N. (2019). Direct and Oriented Conversion of CO_2 into Value-Added Aromatics. Chemistry (Basel). *25*, 5149–5153.
61. Ni, Y., Chen, Z., Fu, Y., Liu, Y., Zhu, W., and Liu, Z. (2018). Selective conversion of CO2 and H2 into aromatics. Nat. Commun. *9*, 3457.
62. Wei, J., Ge, Q., Yao, R., Wen, Z., Fang, C., Guo, L., Xu, H., and Sun, J. (2017). Directly converting CO_2 into a gasoline fuel. Nat. Commun. *8*, 15174.
63. Liu, X., Wang, M., Yin, H., Hu, J., Cheng, K., Kang, J., Zhang, Q., and Wang, Y. (2020). Tandem Catalysis for Hydrogenation of CO and CO_2 to Lower Olefins with Bifunctional Catalysts Composed of Spinel Oxide and SAPO-34. ACS Catal. *10*, 8303–8314.
64. Ramirez, A., Gevers, L., Bavykina, A., Ould-Chikh, S., and Gascon, J. (2018). Metal Organic Framework-Derived Iron Catalysts for the Direct Hydrogenation of CO_2 to Short Chain Olefins. ACS Catal. *8*, 9174–9182.
65. Gao, P., Dang, S., Li, S., Bu, X., Liu, Z., Qiu, M., Yang, C., Wang, H., Zhong, L., Han, Y., et al. (2017). Direct Production of Lower Olefins from CO_2 Conversion via Bifunctional Catalysis. ACS Catal. *8*, 571–578.
66. Li, Z., Wang, J., Qu, Y., Liu, H., Tang, C., Miao, S., Feng, Z., An, H., and Li, C. (2017). Highly Selective Conversion of Carbon Dioxide to Lower Olefins. ACS Catal. *7*, 8544–8548.
67. Xu, D., Ding, M., Hong, X., and Liu, G. (2020). Mechanistic Aspects of the Role of K Promotion on Cu–Fe-Based Catalysts for Higher Alcohol Synthesis from CO_2 Hydrogenation. ACS Catal. *10*, 14516–14526.
68. Rabie, A.M., Betiha, M.A., and Park, S.-E. (2017). Direct synthesis of acetic acid by simultaneous co-activation of methane and CO_2 over Cu-exchanged ZSM-5 catalysts. Appl. Catal. B *215*, 50–59.
69. Zhu, J., Diao, T., Wang, W., Xu, X., Sun, X., Carabineiro, S.A., and Zhao, Z. (2017). Boron doped graphitic carbon nitride with acid-base duality for cycloaddition of carbon dioxide to epoxide under solvent-free condition. Appl. Catal., B *219*, 92–100.
70. Zhang, F., Zeng, M., Yappert, R.D., Sun, J., Lee, Y.H., LaPointe, A.M., Peters, B., Abu-Omar, M.M., and Scott, S.L. (2020). Polyethylene upcycling to long-chain alkylaromatics by tandem hydrogenolysis/aromatization. Sci *370*, 437–441.
71. Li, H., Shang, J., Ai, Z., and Zhang, L. (2015). Efficient Visible Light Nitrogen Fixation with BiOBr Nanosheets of Oxygen Vacancies on the Exposed {001} Facets. J. Am. Chem. Soc. *137*, 6393–6399.
72. Chen, F., Huang, H., Ye, L., Zhang, T., Zhang, Y., Han, X., and Ma, T. (2018). Thickness-Dependent Facet Junction Control of Layered $BiOIO_3$ Single Crystals for Highly Efficient CO_2 Photoreduction. Adv. Funct. Mater. *28*.
73. Wang, W., Zhou, H., Liu, Y., Zhang, S., Zhang, Y., Wang, G., Zhang, H., and Zhao, H. (2020). Formation of B-N-C Coordination to Stabilize the Exposed Active Nitrogen Atoms in g-C_3N_4 for Dramatically Enhanced Photocatalytic Ammonia Synthesis Performance. Small *16*, 1906880.
74. Zeng, X., Liu, Y., Xia, Y., Uddin, M.H., Xia, D., McCarthy, D.T., Deletic, A., Yu, J., and Zhang, X. (2020). Cooperatively Modulating Reactive Oxygen Species Generation and Bacteria-photocatalyst Contact over Graphitic Carbon Nitride by Polyethylenimine for Rapid Water Disinfection. Appl. Catal., B *274*, 119095.
75. Gao, R., Cheng, B., Fan, J., Yu, J., and Ho, W. (2021). ZnxCd1–xS quantum dot with enhanced photocatalytic H_2-production performance. Chin. J. Catal. *42*, 15–24.
76. Brown, K.A., Harris, D.F., Wilker, M.B., Rasmussen, A., Khadka, N., Hamby, H., Keable, S., Dukovic, G., Peters, J.W., Seefeldt, L.C., and King, P.W. (2016). Light-driven dinitrogen reduction catalyzed by a CdS: nitrogenase MoFe protein biohybrid. Science *352*, 448–450.
77. Xu, Q., Zhang, L., Cheng, B., Fan, J., and Yu, J. (2020). S-scheme heterojunction photocatalyst. Chem *6*, 1543–1559.
78. Low, J., Jiang, C., Cheng, B., Wageh, S., Al-Ghamdi, A.A., and Yu, J. (2017). A review of direct Z-scheme photocatalysts. Small Methods *1*, 1700080.
79. Liu, X., Liu, H., Wang, Y., Yang, W., and Yu, Y. (2021). Nitrogen-rich g-C_3N_4@AgPd Mott-Schottky heterojunction boosts photocatalytic hydrogen production from water and tandem reduction of NO^{3-} and NO^{2-}. J. Colloid Interface Sci. *581*, 619–626.
80. Jiang, M.-P., Huang, K.-K., Liu, J.-H., Wang, D., Wang, Y., Wang, X., Li, Z.-D., Wang, X.-Y., Geng, Z.-B., Hou, X.-Y., and Feng, S.-H. (2020). Magnetic-Field-Regulated TiO2 {100} Facets: A Strategy for C-C Coupling in CO_2 Photocatalytic Conversion. Chem *6*, 2335–2346.
81. Yuan, L., Li, Y.-H., Tang, Z.-R., Gong, J., and Xu, Y.-J. (2020). Defect-promoted visible light-driven C-C coupling reactions pairing with CO_2 reduction. J. Catal. *390*, 244–250.
82. Dai, Y., Li, C., Shen, Y., Lim, T., Xu, J., Li, Y., Niemantsverdriet, H., Besenbacher, F., Lock, N., and Su, R. (2018). Light-tuned selective photosynthesis of azo- and azoxy-aromatics using graphitic C_3N_4. Nat. Commun. *9*, 60.
83. Qi, M.-Y., Li, Y.-H., Anpo, M., Tang, Z.-R., and Xu, Y.-J. (2020). Efficient Photoredox-Mediated C–C Coupling Organic Synthesis and Hydrogen Production over Engineered Semiconductor Quantum Dots. ACS Catal. *10*, 14327–14335.
84. Zhang, M., Wang, Y., Zhang, Y., Song, J., Si, Y., Yan, J., Ma, C., Liu, Y.T., Yu, J., and Ding, B. (2020). Conductive and Elastic TiO_2 Nanofibrous Aerogels: A New Concept toward Self-Supported Electrocatalysts with Superior Activity and Durability. Angew. Chem. Int. Ed. *59*, 23252–23260.
85. Sun, R., Yin, H., Zhang, Z., Wang, Y., Liang, T., Zhang, S., and Jing, L. (2021). Graphene-Modulated PDI/g-C_3N_4 All-Organic S-Scheme Heterojunction Photocatalysts for Efficient CO_2 Reduction under Full-Spectrum Irradiation. J. Phys. Chem. C *125*, 23830–23839.
86. Liang, H., Zou, H., and Hu, S. (2017). Preparation of the $W_{18}O_{49}$/g-C_3N_4 heterojunction catalyst with full-spectrum-driven photocatalytic N_2 photofixation ability from the UV to near infrared region. New J. Chem. *41*, 8920–8926.
87. Wang, Y., Xing, Z., Zhao, H., Song, S., Liu, M., Li, Z., and Zhou, W. (2022). MoS_2@In_2S_3/Bi_2S_3 Core-shell dual Z-scheme tandem heterojunctions with Broad-spectrum response and enhanced Photothermal-photocatalytic performance. Chem. Eng. J. *431*, 133355.
88. Huang, M., Wang, T., Wu, Z., Shang, Y., Zhao, Y., and Li, B. (2022). Rational fabrication of cadmium-sulfide/graphitic-carbon-nitride/hematite photocatalyst with type II and Z-scheme tandem heterojunctions to promote photocatalytic

carbon dioxide reduction. J. Colloid Interface Sci. *628*, 129–140.

89. Wang, P., Wang, T., Pei, W., Li, F., Yang, Y., Yu, H., and Dong, X. (2023). Bi-function of photocatalytic Cr(VI) removal and monitoring acetone gas by one-dimensional hierarchical TiO_2 @polyoxometalates@MoS_2 tandem heterojunctions. Sensor. Actuator. B Chem. *387*, 133743.
90. Yao, T., An, X., Han, H., Chen, J.Q., and Li, C. (2018). Photoelectrocatalytic Materials for Solar Water Splitting. Adv. Energy Mater. *8*, 1800210.
91. Xie, Q., He, W., Liu, S., Li, C., Zhang, J., and Wong, P.K. (2020). Bifunctional S-scheme g-C_3N_4/Bi/$BiVO_4$ hybrid photocatalysts toward artificial carbon cycling. Chinese J Catal *41*, 140–153.
92. Wang, J., Wang, G., Cheng, B., Yu, J., and Fan, J. (2021). Sulfur-doped g-C_3N_4/TiO_2 S-scheme heterojunction photocatalyst for Congo Red photodegradation. Chin. J. Catal. *42*, 56–68.
93. Patnaik, S., Sahoo, D.P., and Parida, K.M. (2020). Bimetallic co-effect of Au-Pd alloyed nanoparticles on mesoporous silica modified g-C_3N_4 for single and simultaneous photocatalytic oxidation of phenol and reduction of hexavalent chromium. J. Colloid Interface Sci. *560*, 519–535.
94. Sun, D., Jang, S., Yim, S.-J., Ye, L., and Kim, D.-P. (2018). Metal Doped Core-Shell Metal-Organic Frameworks@Covalent Organic Frameworks (MOFs@COFs) Hybrids as a Novel Photocatalytic Platform. Adv. Funct. Mater. *28*, 1707110.
95. Wang, J., Jiang, J., Li, D., Meng, X., Zhan, G., Wang, Y., Zhang, A., Sun, Y., Ruan, R., and Ragauskas, A.J. (2022). Creating values from wastes: Producing biofuels from waste cooking oil via a tandem vapor-phase hydrotreating process. Appl. Energy *323*, 119629.
96. Biswas, A.N., Xie, Z., Xia, R., Overa, S., Jiao, F., and Chen, J.G. (2022). Tandem Electrocatalytic–Thermocatalytic Reaction Scheme for CO_2 Conversion to C3 Oxygenates. ACS Energy Lett. *7*, 2904–2910.
97. Zhang, W., Xi, D., Chen, Y., Chen, A., Jiang, Y., Liu, H., Zhou, Z., Zhang, H., Liu, Z., Long, R., and Xiong, Y. (2023). Light-driven flow synthesis of acetic acid from methane with chemical looping. Nat. Commun. *14*, 3047.
98. Xu, L., Zhang, Y., Zivkovic, V., and Zheng, M. (2022). Deacidification of high-acid rice bran oil by the tandem continuous-flow enzymatic reactors. Food Chem. *393*, 133440.
99. Deng, J., Cai, Y., Chen, J., Wang, Q., Lu, J., Chen, X., Zhang, W., Wu, K., Wang, W., Wei, L., et al. (2023). Towards Automated Microfluidic-based Platforms: Optimizing Hydrogenation Efficiency of Nitrobenzene through π–π Interactions in Pd Nanoparticles on Covalent Organic Frameworks. Angew. Chem. Int. Ed. *62*, e202302297.
100. Ithisuphalap, K., Zhang, H., Guo, L., Yang, Q., Yang, H., and Wu, G. (2018). Photocatalysis and Photoelectrocatalysis Methods of Nitrogen Reduction for Sustainable Ammonia Synthesis. Small Methods *3*, 1800352.
101. Meng, X., Liu, L., Ouyang, S., Xu, H., Wang, D., Zhao, N., and Ye, J. (2016). Nanometals for Solar-to-Chemical Energy Conversion: From Semiconductor-Based Photocatalysis to Plasmon-Mediated Photocatalysis and Photo-Thermocatalysis. Adv. Mater. *28*, 6781–6803.
102. Liang, C., Lu, Z.-A., Wu, J., Chen, M.-X., Zhang, Y., Zhang, B., Gao, G.-L., Li, S., and Xu, P. (2020). Recent Advances in Plasmon-Promoted Organic Transformations Using Silver-Based Catalysts. ACS Appl. Mater. Interfaces *12*, 54266–54284.
103. Li, P., Liu, L., An, W., Wang, H., Guo, H., Liang, Y., and Cui, W. (2020). Ultrathin porous g-C_3N_4 nanosheets modified with AuCu alloy nanoparticles and C-C coupling photothermal catalytic reduction of CO to ethanol. Appl. Catal., B *266*, 118618.